

# Very Magnetized White Dwarfs with Axisymmetric Magnetic Field and the Importance of the Electron Capture and Pycnonuclear Fusion Reactions for their Stability

Edson Otoniel<sup>1,3,\*</sup> Bruno Franzon<sup>2,†</sup> Manuel Malheiro<sup>1,‡</sup> Stefan Schramm<sup>2,§</sup> and Fridolin Weber<sup>3,¶</sup>

<sup>1</sup>*Departamento de Física, Instituto Tecnológico de Aeronáutica, Praça Marechal Eduardo Gomes, 50 - Vila das Acácias, 12228-900 São José dos Campos, SP, Brazil*

<sup>2</sup>*Frankfurt Institute for Advanced Studies, Ruth-Moufang-1 60438 Frankfurt am Main, Germany and*

<sup>3</sup>*Department of Physics, San Diego State University,*

*5500 Campanile Drive, San Diego, California 92182, USA and*

*Center for Astrophysics and Space Sciences, University of California at San Diego, La Jolla, California 92093, USA*

(Dated: July 11, 2018)

In this work, we study the properties of magnetized white dwarfs taking into account possible instabilities due to electron capture and pycnonuclear fusion reactions in the cores of such objects. The structure of white dwarfs is obtained by solving the Einstein-Maxwell equations with a poloidal magnetic field in a fully general relativistic approach. The stellar interior is composed of a regular crystal lattice made of carbon ions immersed in a degenerate relativistic electron gas. The onsets of electron capture reactions and pycnonuclear reactions are determined with and without magnetic fields. We find that magnetized white dwarfs violate the standard Chandrasekhar mass limit significantly, even when electron capture and pycnonuclear fusion reactions are present in the stellar interior. We obtain a maximum white dwarf mass of around  $2.14 M_{\odot}$  for a central magnetic field of  $\sim 3.85 \times 10^{14}$  G, which indicates that magnetized white dwarfs may play a role for the interpretation of superluminous type Ia supernovae. Furthermore, we show that the critical density for pycnonuclear fusion reactions limits the central white dwarf density to  $9.35 \times 10^9$  g/cm<sup>3</sup>. As a result, equatorial radii of white dwarfs cannot be smaller than  $\sim 1100$  km. Another interesting feature concerns the relationship between the central stellar density and the strength of the magnetic field at the core of a magnetized white dwarf. For high magnetic fields, we find that the central density increases (stellar radius decrease) with magnetic field strength, which makes ultramagnetized white dwarfs more compact. The opposite is the case, however, if the central magnetic field is less than  $\sim 10^{13}$  G. In the latter case, the central density decreases (stellar radius increases) with central magnetic field strengths.

arXiv:1609.05994v2 [astro-ph.SR] 29 Mar 2017

---

\* edson.otoniel@gmail.com

† franzon@fias.unifrankfurt.de

‡ malheiro@ita.br

§ schramm@fias.unifrankfurt.de

¶ fweber@mail.sdsu.edu

## I. INTRODUCTION

It is generally accepted that stars born with masses below around 10 solar masses end up their evolutions as white dwarfs (WDs) [1–3]. With a typical composition mostly made of carbon, oxygen, or helium, white dwarfs possess central densities up to  $\sim 10^{11}$  g/cm<sup>3</sup>. They can be very hot [4], fast rotating [5–7] and strongly magnetized [8–10]. The observed surface magnetic fields range from  $10^6$  G to  $10^9$  G [11–16]. The internal magnetic fields of white dwarfs are not known, but they are expected to be larger than their surface magnetic fields. This is due to the fact that in ideal magneto hydrodynamics (MHD), the magnetic field,  $B$ , is ‘frozen-in’ with the fluid and  $B \propto \rho$ , with  $\rho$  being the local mass density (see, e.g., Refs. [17, 18]). A simple estimate of the internal magnetic field strength follows from the virial theorem by equating the magnetic field energy with the gravitational binding energy, which leads to an upper limit for the magnetic fields inside WDs of about  $\sim 10^{13}$  G. On the other hand, analytic and numeric calculations, both in Newtonian theory as well as in General Relativity theory, show that WDs may have internal magnetic fields as large as  $10^{12-16}$  G (see, e.g., Refs. [2, 16, 19–24]).

The relationship between the gravitational stellar mass,  $M$ , and the radius,  $R$ , of non-magnetized white dwarfs was first determined by Chandrasekhar [25]. Recently, mass-radius relationships of magnetic white dwarfs have been discussed in the literature (see, e.g., Refs. [20, 22, 26]). These studies show that the masses of white dwarfs increase in the presence of strong magnetic fields. This is due to the Lorentz force, which acts against gravity, therefore supporting stars with higher masses.

Based on recent observations of several superluminous type Ia supernovae (SN 2006gz, SN 2007if, SN 2009dc, SN 2003fg) [27–33], it has been suggested that the progenitor masses of such supernovae significantly exceed the Chandrasekhar mass limit of  $M_{\text{Ch}} \sim 1.4 M_{\odot}$  [34]. Super-heavy progenitors were studied as a result of mergers of two massive white dwarfs [35–37]. Alternatively, the authors of Ref. [38] obtained super-Chandrasekhar white dwarfs for magnetically charged stars. In addition, super-Chandrasekhar white dwarfs were investigated in the presence of strong magnetic fields in Refs. [39]. In Refs. [40, 41], WDs models with magnetic fields were calculated in the framework of Newtonian physics. A recent study of differential rotating, magnetized white dwarfs has shown that differential rotation might increase the mass of magnetized white dwarfs up to  $3.1 M_{\odot}$  [42]. Also, as shown in Ref. [43], purely toroidal magnetic field components can increase the masses of white dwarfs up to  $5 M_{\odot}$ .

According to Refs. [44], effects of an extremely large and uniform magnetic field on the equation of state (EOS) of a white dwarf could increase its critical mass up to  $2.58 M_{\odot}$ . This mass limit is reached for extremely large magnetic fields of  $\sim 10^{18}$  G. Nevertheless, as already discussed in Refs. [45, 46], the breaking of spherical symmetry due to magnetic fields and micro-physical effects, such as electron capture reactions and pycnonuclear reactions, can severely limit the magnetic field inside white dwarfs.

In Ref. [22], mass-radius relationships of highly magnetized white dwarfs were computed using a pure degenerate electron Fermi gas. However, according to Ref. [47], many-body corrections modify the EOS and, therefore, the mass-radius relationship of white dwarfs. The purpose of our paper is two-fold. Firstly, we model white dwarfs using a model for the equation of state which takes into account not only the electron Fermi gas contribution, but also the contribution from electron-ion interactions [48]. Secondly, we perform a stability analysis of the matter in the cores of white dwarfs against electron capture and pycnonuclear fusion reactions. The Landau energy levels of electrons are modified by relativistic effects if the magnetic field strength is higher than the critical QED magnetic field strength of  $B_{\text{cr}} = 4.4 \times 10^{13}$  G. However, as already shown in Ref. [49], the global properties of white dwarfs, such as masses and the radii, are nearly independent of Landau quantization. For this reason, we do not take into account magnetic fields effects in the equation of state to calculate the global properties of WD’s.

Our paper is organized as follows. In Sec. II, we discuss the stellar interior of white dwarfs and details of the equation of state used in our study to model white dwarfs. This is followed, in Sec. III, by a brief discussion of the equations that are being solved numerically to obtain the structure of stationary magnetized white dwarfs. In Sec. IV, we briefly discuss the Einstein-Maxwell tensor and the metric tensor used to solve Einstein’s field equations of General Relativity. The results of our study are discussed in Sec. V and summarized in Sec. VI.

## II. STELLAR INTERIOR

The properties of fermionic matter have been studied many decades ago in Refs. [47, 50]. Typically, a white dwarf is composed of atomic nuclei immersed in a fully ionized electron gas. In this work, we make use of the latest experimental atomic mass data [51, 52] used to determine the equation of state. Modifications of the equation of state due to the interactions between electrons and atomic nuclei are taken into account too. The model adopted to describe the nuclear lattice was derived for the outer crust of a neutron star in Refs. [46, 53] and later applied to WDs in Ref. [54]. According to Ref. [54], the cores of white dwarfs are subjected to the degenerate electron and ionic

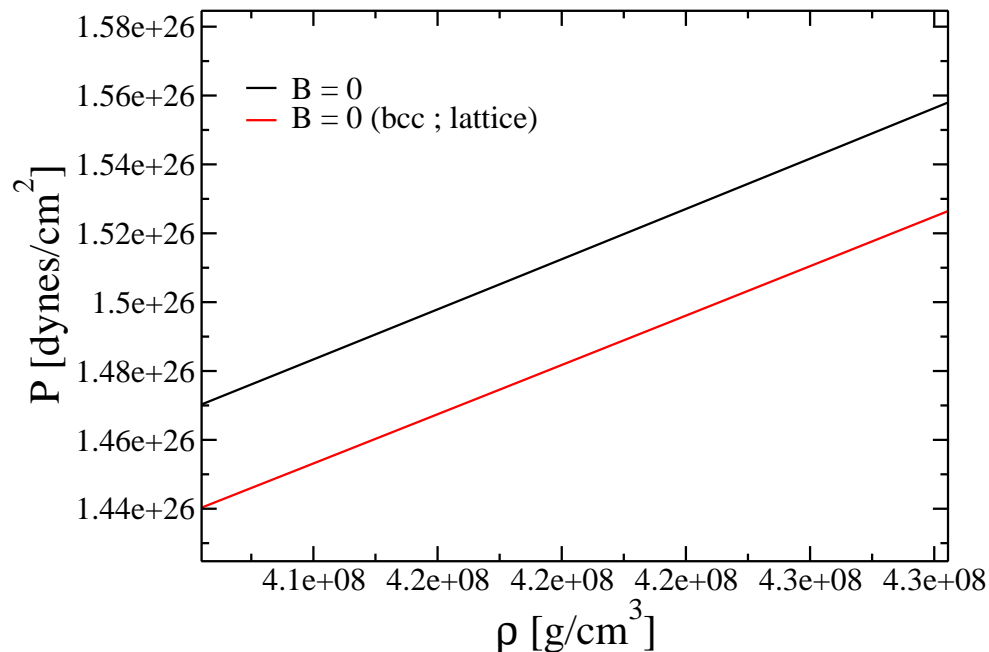


FIG. 1. (Color online) Equation of state for  $B = 0$  with (red curve) and without (black curve) lattice contributions.

lattice pressures. The total pressure is then given by

$$P = P_e + P_L(Z, Z'), \quad (1)$$

where  $P_e$  denotes the electron pressure, determined in [47], and  $P_L(Z, Z')$  is the lattice pressure for two different type of ions. The lattice pressure is given by the energy density of the ionic lattice (see Ref. [53]),

$$P_L(Z, Z') = \frac{1}{3} \mathcal{E}_L, \quad (2)$$

with  $Z$  and  $Z'$  being the proton number of two different ions. In our case, the white dwarf is composed of carbon ions, i.e.,  $Z'=Z=12$ . Following the Bohr-van Leeuwen theorem [53], the lattice pressure of ions arranged in a regular body-centered-cubic (bcc) crystal does not depend on the magnetic field, apart from a small contribution due to the quantum zero-point motion of ions. In this case, the lattice energy density reads [46]

$$\mathcal{E}_L = C e^2 n_e^{4/3} G(Z, Z'), \quad (3)$$

with  $G(Z, Z')$  given by

$$G(Z, Z') = \frac{\alpha Z^2 + \gamma Z'^2 + (1 - \alpha - \gamma) Z Z'}{(\xi Z + (1 - \xi) Z')^{4/3}}. \quad (4)$$

The quantities  $C$ ,  $\alpha$ ,  $\gamma$  are lattice constants and  $\xi$  is the ratio of ions  $\frac{A}{Z}Y$  and  $\frac{A'}{Z'}Y$  in the lattice [54] (see also Table I). If only a single ion is present in the lattice, Eq. 4 does not depend on  $\alpha$  and  $\gamma$  so that Eq. (3) becomes

$$\mathcal{E}_L = C e^2 n_e^{4/3} Z^{2/3}, \quad (5)$$

The energy density is given in terms of the degenerate electron energy, the energy density of the ions, and the energy density of the ionic lattice,

$$\mathcal{E} = n_x M(Z, A) c^2 + n_{x'} M(Z', A') c^2 + \mathcal{E}_e + \mathcal{E}_L - n_e m_e c^2, \quad (6)$$

where  $n_x$  and  $n_{x'}$  are the number densities of atomic nuclei with masses  $M(Z, A)$  and  $M(Z', A')$ , respectively. As already mentioned above, here we adopt the most recent experimental values for  $M$  (see Refs. [51, 52]).

Figure 1 shows the impact of lattice contributions on the white dwarf equation of state studied in this paper. The black lines (no lattice contribution) and red dashed line (with lattice contribution) are for white dwarf matter with zero magnetic field ( $B = 0$ ). One sees that adding the lattice contribution to the equation of state lowers the pressure somewhat, which in turn makes white dwarfs less massive. It also follows from this figure that the presence of lattice contributions reduces the radii of white dwarfs (renders them more compact) with comparable central pressures.

TABLE I. Lattice constants  $C$ ,  $\alpha$ ,  $\gamma$  and parameters  $(1 - \alpha - \gamma)$  and  $\xi$  for a body-centered-cubic (bcc) structure, as obtained by the method of Coldwell-Horsfall and Maradudin (see Ref. [54]) for more details.

Lattice	$C$	$\alpha$	$\gamma$	$(1 - \alpha - \gamma)$	$\xi$
bcc	-1.444231	0.389821	0.389821	0.220358	0.5

### III. INSTABILITIES IN STRONGLY MAGNETIZED WHITE DWARFS

#### A. Inverse $\beta$ decay

As shown in Refs. [54, 55], the matter inside of white dwarfs is unstable due to inverse  $\beta$ -decay,

$$A(N, Z) + e^- \rightarrow A(N + 1, Z - 1) + \nu_e.$$

Because of this reaction, atomic nuclei become more neutron rich and the energy density of the matter is being reduced, at a given pressure, leading to a softer EoS. Using the thermodynamic relation (at zero temperature)  $\mathcal{E}_e + P_e = n_e \mu_e$ , one obtains the Gibbs free energy,  $g$ , per nucleon as

$$g(Z, Z') = mc^2 + \frac{\xi}{\xi A + (1 - \xi)A'} \Delta(A, Z) + \frac{(1 - \xi)}{\xi A + (1 - \xi)A'} \Delta(A', Z') + \gamma_e \left[ \mu_e + m_e c^2 + \frac{4}{3} \frac{\mathcal{E}_L}{n_e} \right], \quad (7)$$

with  $m$  being the neutron mass and  $\Delta(A, Z)$  denoting the excess mass of nuclei, which, for magnetic field strengths  $< 10^{17}$  G, is independent of the magnetic field, see, e.g., Ref [46]. For  $\gamma_e = \bar{Z}/A$  we have  $\bar{Z} = \xi Z + (1 - \xi)Z'$  and  $\bar{A} = \xi A + (1 - \xi)A'$ , with  $\mu_e$  being the electron chemical potential. Inverse  $\beta$ -decay reactions are believed to occur in the cores of white dwarfs if the condition [54]

$$g(Z, Z') \geq g(Z - \Delta Z, Z' - \Delta Z') \quad (8)$$

is fulfilled, where  $g(Z, Z')$  and  $g(Z - \Delta Z, Z' - \Delta Z')$  follow from Eq. (7) and the possible choices for  $\Delta Z$  and  $\Delta Z'$  are  $\Delta Z = 1$  &  $\Delta Z' = 0$ ,  $\Delta Z = 0$  &  $\Delta Z' = 1$ , and  $\Delta Z = 1$  &  $\Delta Z' = 1$ .

From the inequality (8), we obtain the following relation

$$\Delta \bar{Z} \left[ \mu_e + \frac{4}{3} C e^2 n_e^{1/3} \Delta(\bar{Z} G(Z, Z')) \right] \geq \bar{\mu}_e^\beta \quad (9)$$

with the electron number density  $n_e$  and mass density  $\rho$  of a magnetized electron gas given respectively by

$$n_e = \frac{2B_\star}{(2\pi)^2 \lambda^3} \sum_\nu g_{\nu 0} \sqrt{x_F^2 - 1 - 2\nu B_\star}. \quad (10)$$

$$\rho = \frac{1}{\gamma_e} m n_e. \quad (11)$$

where only the ground-state Landau level  $\nu = 0$  is occupied,  $\nu_{\max} = 1$ . For two occupied levels,  $\nu = 0$  and  $\nu = 1$ , one has  $\nu_{\max} = 2$ , and similarly for the higher levels. The quantities  $x_F$  in Eq. (11) and  $\bar{\mu}_e^\beta$  in Eq. (9) are defined as  $x_F \equiv p_F/m_e c$  and

$$\bar{\mu}_e^\beta = \xi \mu_e^\beta(A, Z) + (1 - \xi) \mu_e^\beta(A', Z'), \quad (12)$$

with  $\mu_e^\beta(A, Z)$  and  $\mu_e^\beta(A', Z')$  given by

$$\mu_e^\beta(A, Z) \equiv \Delta(A, Z - \Delta Z) - \Delta(A, Z) + m_e c^2 \quad (13)$$

$$\mu_e^\beta(A', Z') \equiv \Delta(A', Z' - \Delta Z') - \Delta(A', Z') + m_e c^2. \quad (14)$$

Another important quantity is  $\Delta \bar{Z} G(Z, Z')$ , which describes the difference of  $G$ , defined in Eq. (4), before and after an inverse  $\beta$  decay reaction. It is given by

$$\Delta(\bar{Z} G(Z, Z')) = G(Z, Z') - G(Z - \Delta, Z' - \Delta). \quad (15)$$

For an electron gas consisting of only one type of ion, we have

$$\Delta(\bar{Z} G(Z, Z)) = Z^{5/3} - (Z - 1)^{5/3} - \frac{2}{3} Z^{2/3}. \quad (16)$$

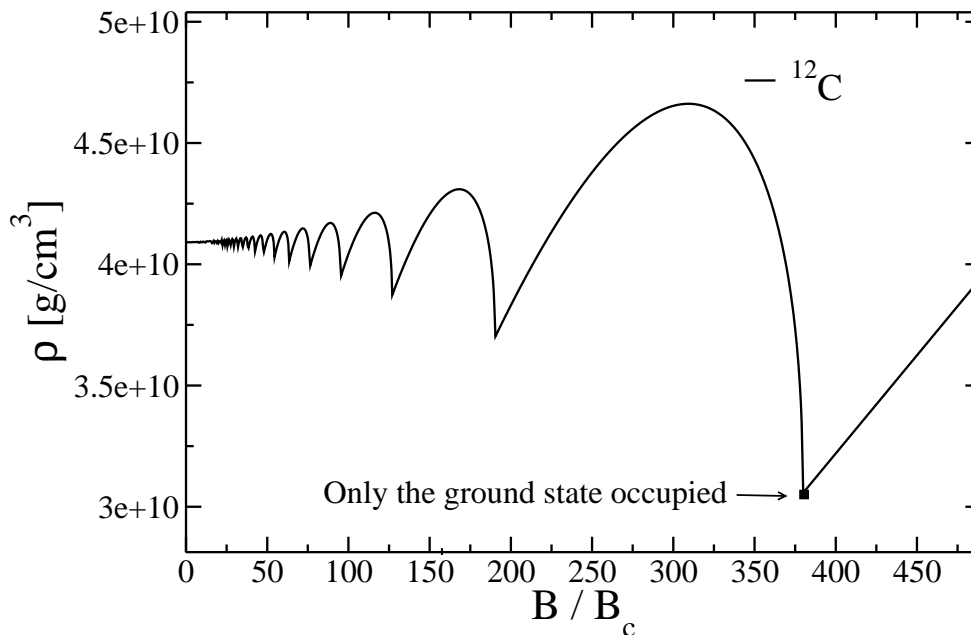


FIG. 2. Mass density thresholds for the onset of electron capture as a function of magnetic field strength (in units of the critical magnetic field,  $B_c$ ), computed from Eq. (9) for matter made of only carbon ions.

In the limit where only the ground state ( $\nu = 0$ ) is fully occupied by electrons, one has

$$n_e = n_{eB} \propto B_\star^{2/3},$$

where  $B_\star = B/B_c$  with  $B_c = 4.414 \times 10^{13}$  G being the critical magnetic field (see Ref. [56] for more details about  $n_{eB}$ ). The chemical potential of the electrons in this case is given by

$$\mu_e \approx \frac{2\pi^2 m_e c^2 \lambda_e^3 n_{eB}}{B_\star}, \quad (17)$$

where  $\lambda_e = \hbar/m_e c$  denotes the Compton wavelength of electrons. In Ref. [54] it was estimated that the maximum magnetic field inside of white dwarfs, before the onset of  $\beta$ -inverse reactions, is given by

$$B_\star^\beta \approx \frac{1}{2} \left( \frac{\bar{\mu}_e^\beta(A, Z)}{m_e c^2 \Delta \bar{Z}} \right)^2 \left[ 1 + \left( \frac{4}{\pi} \right)^{2/3} \frac{C\alpha}{3} \Delta(\bar{Z}G(Z, Z')) \right]^{-2}, \quad (18)$$

with  $\alpha = e^2/(\hbar c)$  the fine structure constant. We note that because of the second term on the right-hand-side of Eq. (18), which originates from lattice contributions, the maximum value of  $B_\star^\beta$  increases if lattice contributions are taken into account.

In Fig. 2 we show the numerical solution of Eq. (9) for white dwarf matter made of only carbon ions immersed in a magnetized electron gas. The oscillatory behavior is caused by the Landau level contributions to the number density, given by Eq. (11). For high values of  $B$  with only the ground state occupied, the dependence of density on  $B$  becomes linear, as can be seen in Fig. 2.

## B. Pycnonuclear reaction

In this section, we will focus on nuclear fusion reactions (pycnonuclear fusion reactions) among heavy atomic nuclei  ${}^A_Z Y$ , schematically expressed as  ${}^A_Z Y + {}^A_Z Y \rightarrow {}^{2A}_{2Z} Y$ . An example of such a reaction is carbon on carbon,  ${}^{12}\text{C} + {}^{12}\text{C}$ . Pycnonuclear reactions have been found to occur over a significant range of stellar densities (see, for instance, Ref. [57]), including the density range found in the interiors of white dwarfs [46, 54]. The nuclear fusion rates at which pycnonuclear reactions proceed, however, are highly uncertain because of some poorly constrained parameters

(see Ref. [57, 58]). The reaction rates have been calculated for different models. In Ref. [57], the pycnonuclear reaction rates are defined as

$$R_{\text{pyc}} = \frac{n_i}{2} S(E_{\text{pk}}) \frac{\hbar}{mZ^2e^2} P_{\text{pyc}} F_{\text{pyc}} \quad (19)$$

where  $S(E_{\text{pk}})$  is the astrophysical S-factor used in Ref. [57] for the NL2 nuclear model parametrization. According to Ref. [57], an analytic equation for the S-factor is given by

$$S(E_{\text{pk}}) = 5.15 \times 10^{16} \exp \left[ -0.428 E_{\text{pk}} - \frac{3E_{\text{pk}}^{0.308}}{1 + e^{0.613(8-E_{\text{pk}})}} \right], \quad (20)$$

where  $S(E_{\text{pk}})$  is in units of MeV barn. The factors  $P_{\text{pyc}}$  and  $F_{\text{pyc}}$  in Eq. (19) are given by

$$P_{\text{pyc}} = \exp \left( -C_{\text{exp}}/\sqrt{\lambda} \right), \quad (21)$$

$$F_{\text{pyc}} = 8C_{\text{pyc}} 11.515/\lambda^{C_{\text{pl}}}, \quad (22)$$

with  $C_{\text{exp}}$ ,  $C_{\text{pyc}}$  and  $C_{\text{pl}}$  are dimensionless parameters for a regular bcc-type crystal lattice (see at zero temperature). Their values are listed in Table II.

TABLE II. Coefficients  $C_{\text{exp}}$ ,  $C_{\text{pyc}}$ ,  $C_{\text{pl}}$  related to pycnonuclear reaction rates at zero temperature, computed for nuclear model NL2 (see Refs. [59, 60]).

Model	$C_{\text{exp}}$	$C_{\text{pyc}}$	$C_{\text{pl}}$
bcc; static lattice	2.638	3.90	1.25

The inverse-length parameter  $\lambda$  in Eq. (21) and Eq. (22) has the form Refs. [57, 58]

$$\lambda = \frac{\hbar^2}{mZ^2e^2} \left( \frac{n_i}{2} \right)^{1/3} = \frac{1}{AZ^2} \left( \frac{1}{A} \frac{\rho X_i}{1.3574 \times 10^{11} \text{g cm}^{-3}} \right)^{1/3}. \quad (23)$$

For number densities  $\rho$  less than neutron drip density one has  $X_i = 1$  [57] and the pycnonuclear reaction rates are given by

$$R_{\text{pyc}} = \rho X_i A Z^4 S(E_{\text{pk}}) C_{\text{pyc}} 10^{46} \lambda^{3-C_{\text{pl}}} \exp \left( -C_{\text{exp}}/\sqrt{\lambda} \right), \quad (24)$$

with  $R_{\text{pyc}}$  given in units of  $\text{cm}^{-3} \text{s}^{-1}$ . The zero-point oscillation energy  $E_{\text{pk}}$  of  $^{12}\text{C}$  nuclei at  $\rho = 10^{10} \text{g/cm}^3$  is given by Ref. [2]

$$E_{\text{pk}} = \hbar\omega = \hbar \left( \frac{4\pi e^2 Z^2 \rho}{A^2 M^2} \right)^{1/2}. \quad (25)$$

The time it takes for the complete fusion of atomic nuclei of mass  $Am$  is obtained from [6, 57]

$$\tau_{\text{pyc}} = \frac{n_x}{R_{\text{pyc}}} = \frac{\rho}{Am R_{\text{pyc}}}. \quad (26)$$

As already mentioned above, the reaction rates are rather uncertain, and the analytic astrophysical S-factor has an uncertainty of  $\sim 3.5$ , which considerably affects the density thresholds of pycnonuclear reaction and their reaction times. Finally, in Fig. 3 we show pycnonuclear fusion reaction rates and pycnonuclear reaction time scales for carbon burning at zero temperature as functions of mass density. The bcc crystal lattice for nuclear model NL2 was employed to produce Fig. 3.

#### IV. WHITE DWARFS WITH AXISYMMETRIC MAGNETIC FIELDS

The numerical technique used in this work to study axisymmetric magnetic fields was first applied to neutron stars in Refs. [61, 62], and more recently in Ref. [63–65]. The same formalism was used to study rotating and magnetized

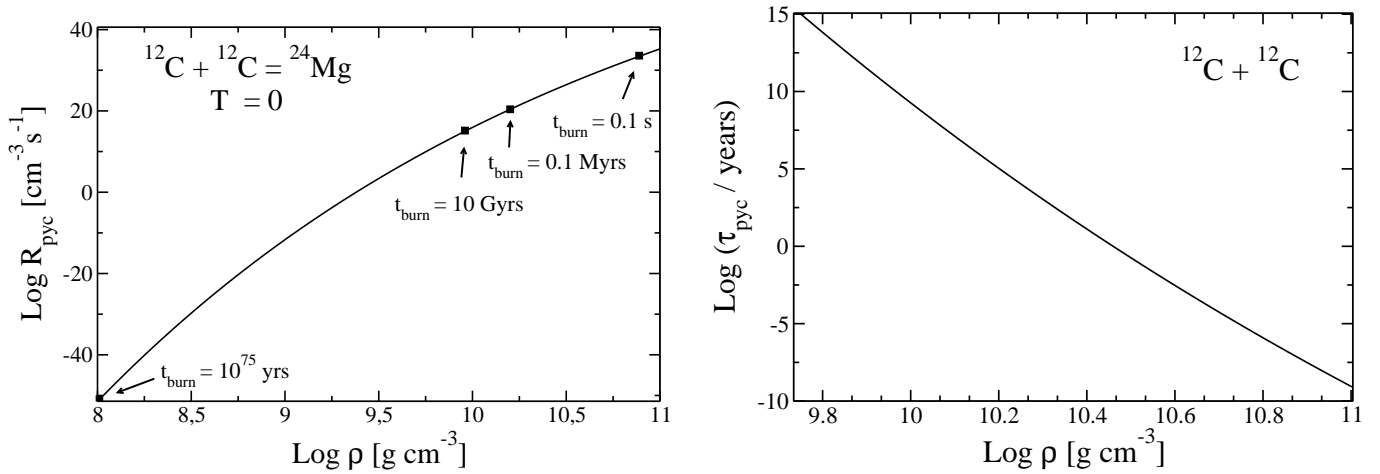


FIG. 3. Left: pycnonuclear fusion reaction rates for carbon burning at zero temperature as functions of mass density, for nuclear model NL2 and a bcc crystal lattice. Right: pycnonuclear reaction time scales at zero temperature for C+C fusion as a function of mass density. The S-factor is given by Eq. (20) and the zero-point oscillation energy is  $E_{pk} \sim 0.034$  MeV.

white dwarfs in Ref. [22]. Here we build stellar equilibrium configurations by solving the Einstein-Maxwell field equations in a fully general relativistic approach. For more details about the theoretical formalism and numerical procedure, see, for instance, Ref. [66]. Below we show the basic electromagnetic equations which, combined with the gravitational equations, are solved numerically by means of a spectral method. In this context, the stress-energy tensor  $T_{\alpha\beta}$  is composed of the matter and the electromagnetic source terms,

$$T_{\alpha\beta} = (e + p)u_\alpha u_\beta + pg_{\alpha\beta} + \frac{1}{\mu_0} \left( F_{\alpha\mu} F_\beta^\mu - \frac{1}{4} F_{\mu\nu} F^{\mu\nu} g_{\alpha\beta} \right). \quad (27)$$

Here  $F_{\alpha\mu}$  is the antisymmetric Faraday tensor defined as  $F_{\alpha\mu} = \partial_\alpha A_\mu - \partial_\mu A_\alpha$ , with  $A_\mu$  denoting the electromagnetic four-potential  $A_\mu = (A_t, 0, 0, A_\phi)$ . The total energy density of the system is  $e$ , the pressure is denoted by  $p$ ,  $u_\alpha$  is the fluid 4-velocity, and the metric tensor is  $g_{\alpha\beta}$ . The first term in Eq. (27) represents the isotropic (ideal) matter contribution to the energy momentum-tensor, while the second term is the anisotropic electromagnetic field contribution.

The metric tensor in axisymmetric spherical-like coordinates  $(r, \theta, \phi)$  can be read of from the line element

$$ds^2 = -N^2 dt^2 + \Psi^2 r^2 \sin^2 \theta (d\phi - N^\phi dt)^2 + \lambda^2 (dr^2 + r^2 d\theta^2), \quad (28)$$

where  $N$ ,  $N^\phi$ ,  $\Psi$  and  $\lambda$  are functions of the coordinates  $(r, \theta)$  [61]. As in Ref. [61], the equation of motion for a star endowed with magnetic fields reads

$$H(r, \theta) + \nu(r, \theta) + M(r, \theta) = \text{const}, \quad (29)$$

where  $H(r, \theta)$  is the heat function defined in terms of the baryon number density  $n$ ,

$$H = \int_0^n \frac{1}{e(n_1) + p(n_1)} \frac{dP}{dn}(n_1) dn_1. \quad (30)$$

The quantity  $\nu(r, \theta)$  in Eq. (29) is defined as  $\nu = \ln N$ , and the magnetic potential  $M(r, \theta)$  is given by

$$M(r, \theta) = M(A_\phi(r, \theta)) \equiv - \int_{A_\phi(r, \theta)}^0 f(x) dx, \quad (31)$$

where  $f(x)$  denotes the current function. Magnetic stellar models are obtained by assuming a constant value,  $f_0$ , for the latter [64]. According to Ref. [62], other choices for  $f(x)$  are possible, but the general conclusions as presented in this work remain the same. The constant current function is a standard way to generate self-consistently a dipolar magnetic field throughout the star.

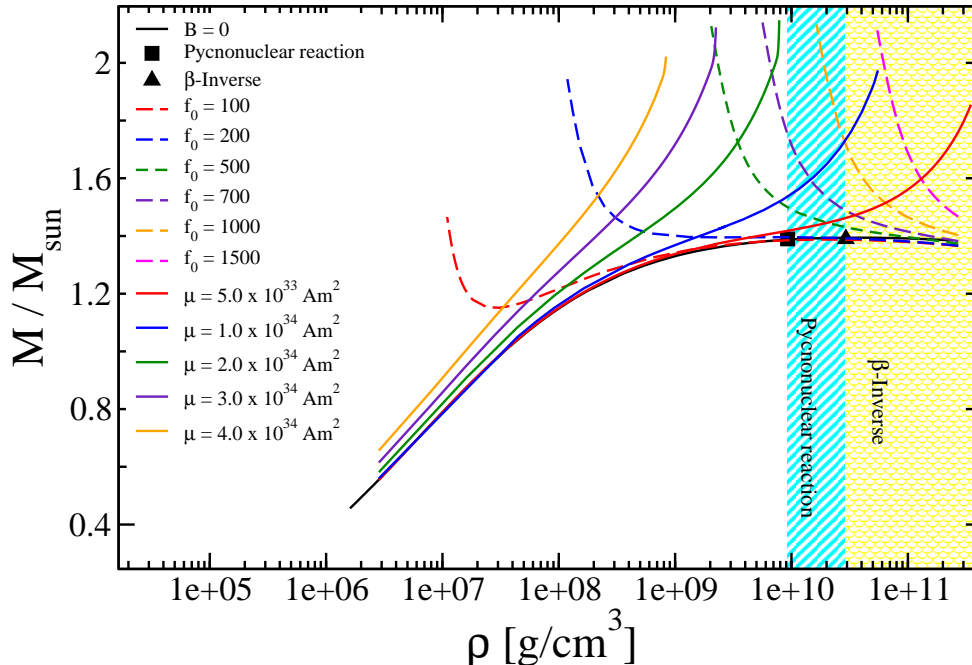


FIG. 4. (Color online) Gravitational mass as a function of central mass density for magnetized white dwarfs, for different values for the current function,  $f_0$ , and magnetic dipole moment,  $\mu$ . Stars located in the colored areas are subject to pycnonuclear reactions and inverse  $\beta$ -decay. The threshold of these reactions are shown in Table III. The solid square and triangle mark the densities at which pycnonuclear and inverse  $\beta$ -decay reactions set in, respectively.

## V. RESULTS

In this section, we discuss the effects of strong magnetic fields on the global properties of stationary white dwarfs taking into account instabilities due to inverse  $\beta$ -decay and pycnonuclear fusion reactions in their cores. In addition, we make use of an equation of state for white dwarf matter that accounts for electron-ion interactions and is computed for the latest experimental atomic mass data. The instabilities related to the microphysics are fundamental since they put constraints on the equilibrium configurations and also limit the maximum magnetic fields which these stars can have [46]. In addition to the magnetic profiles, which have already been computed in Ref. [22], we also compute stellar models at constant magnetic dipole moments  $\mu$ . In Ref. [22], a simple Fermi gas model was used to model white dwarfs, and the microphysical issues were not addressed. In our study, the maximum white dwarf mass for non-magnetized stars is smaller than the one considered in Ref. [22], since the lattice contribution softens the EOS.

In Fig. 4, we show the gravitational mass versus central density of white dwarf sequences computed for different (fixed) magnetic dipole moments,  $\mu$ , and current functions,  $f_0$ . The magnetic dipole moment is defined as (see Ref. [61])

$$\frac{2\mu \cos \theta}{r^3} = B(r) |_{r \rightarrow \infty}, \quad (32)$$

which is the radial (orthonormal) component of the magnetic field of a magnetic dipole seen by an observer at infinity. As can be seen from Fig. 4, a larger magnetic moment  $\mu$  leads first to an increase in the white dwarf maximum mass. However, if we increase  $\mu$  further, the maximum mass begins to drop. This is due to the fact that the stellar radius becomes larger (see also Fig. 5), which reduces the magnetic field (see Eq. 32). As a consequence, the Lorentz force becomes smaller, rendering the maximum mass configurations less massive.

As can be seen in Fig. 4, the masses of magnetized white dwarfs increase monotonically with central density. The behavior is very different if the value of the current function is kept constant, in which case non-monotonic (in some cases even multivalued) mass-density relationships are obtained. The cross-hatched area in Fig. 4 shows the density regime where pycnonuclear fusion reactions become possible. The position of the white dwarf with just the right threshold density ( $9.25 \times 10^9 \text{ g/cm}^3$ ) for this reaction to occur is marked with a solid black square in Fig. 4. The

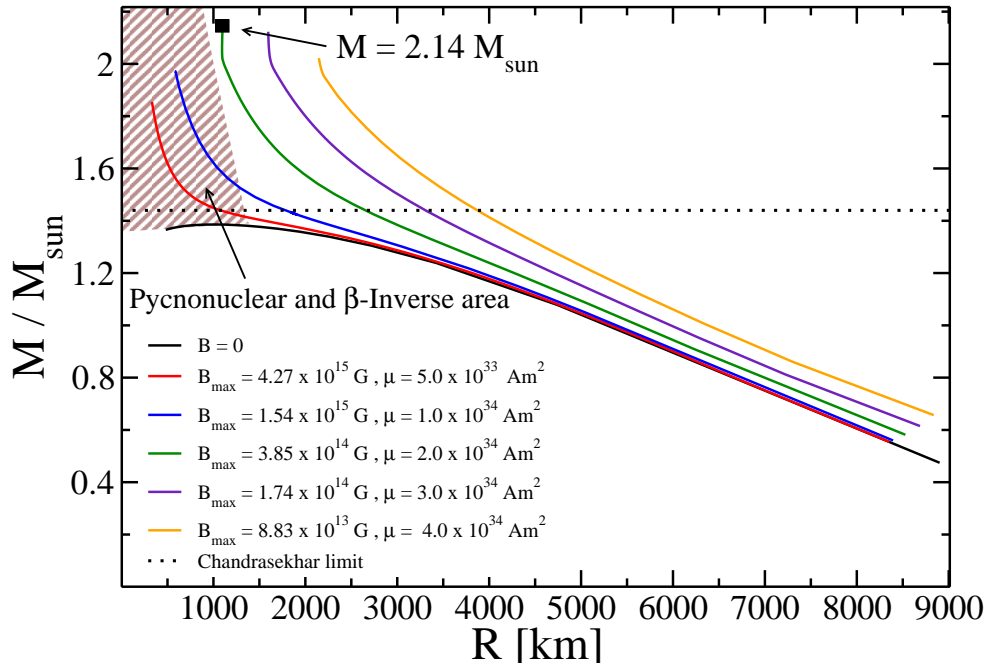


FIG. 5. (Color online) Mass-radius relationship of magnetized white dwarfs for different magnetic dipole moments,  $\mu$ . The black line represents the mass-radius relationship of non-magnetized white dwarfs. The horizontal line represents the Chandrasekhar mass limit for spherical stars. Also shown are the values of the magnetic field  $B_{\max}$  (together with the corresponding magnetic dipole moment  $\mu$ ) at the centers of the respective maximum mass stars (end points of each curve with fixed  $\mu$ ). White dwarfs located in the colored (upper left) corner are subject to pycnonuclear fusion ( $\tau_{\text{pyc}} = 10$  Gyrs) or inverse  $\beta$ -decay reactions.

pycnonuclear reaction time at that density is 10 Gyrs. For a central white dwarf density of  $1.59 \times 10^{10} \text{ g/cm}^3$  the fusion reaction time decreases to 0.1 Myrs (see Fig. 3). White dwarfs subject to inverse  $\beta$ -decay reactions in their cores are located in the yellow area (marked “ $\beta$ -inverse”) of Fig. 4. The most massive stable white dwarf which is not subject to microscopic instability reactions in its core (end point of the curve with  $\mu = 2 \times 10^{34} \text{ Am}^2$ ), has a mass of  $\sim 2.14 M_{\odot}$  and a radius (see Fig. 5) of  $\sim 1096 \text{ km}$ . Finally, we note that the condition  $dM/d\rho_c > 0$  for stability against radial oscillations is fulfilled for all white dwarf sequences for which the magnetic dipole moment is kept fixed, as can be seen in Fig. 4. An overview of the density thresholds discussed just above is provided in Table III for white dwarfs with different magnetic field values and magnetic dipole moments.

TABLE III. Thresholds of inverse  $\beta$ -reactions and pycnonuclear fusion reactions (pycnonuclear reaction time of 10 Gyrs) in carbon white dwarfs for different magnetic fields,  $B$ , and magnetic dipole moments,  $\mu$ .

${}^{12}\text{C}$	$\mu \text{ (Am}^2\text{)}$	$B_{\max} \text{ (G)}$	$\rho_{\text{pyc}} \text{ (g/cm}^3\text{)}$	$\rho_{\beta} \text{ (g/cm}^3\text{)}$
	$5.0 \times 10^{33}$	$4.27 \times 10^{15}$	$9.26 \times 10^9$	$4.00 \times 10^{10}$
	$1.0 \times 10^{34}$	$1.54 \times 10^{15}$	$9.21 \times 10^9$	$4.07 \times 10^{10}$
	$2.0 \times 10^{34}$	$3.85 \times 10^{14}$	$9.24 \times 10^9$	$4.10 \times 10^{10}$
	$3.0 \times 10^{34}$	$1.74 \times 10^{14}$	$9.25 \times 10^9$	$4.10 \times 10^{10}$
	$4.0 \times 10^{34}$	$8.83 \times 10^{13}$	$9.25 \times 10^9$	$4.10 \times 10^{10}$

The mass-radius relationship of magnetized white dwarfs for different magnetic dipole moments  $\mu$  is shown in Fig. 5. One sees that increasing values of  $\mu$  lead to white dwarfs with larger radii, because of the added magnetic field energy. The strength of the magnetic field can be inferred from Fig. 6, which shows the gravitational mass as a function of surface ( $B_s$ ) and central ( $B_c$ ) magnetic fields, the circumferential equatorial radius ( $R_{\text{circ}}$ ), and the baryon number density ( $n_b$ ), for two sample magnetic dipole moments of  $\mu = 0.5 \times 10^{34} \text{ Am}^2$  (red line) and  $\mu = 4.0 \times 10^{34} \text{ Am}^2$  (orange line).

In Fig. 6 (top panels), one sees that the curves with  $\mu = 0.5 \times 10^{34} \text{ Am}^2$  and  $\mu = 4.0 \times 10^{34} \text{ Am}^2$  cross each other. This is due to the fact that the magnetic field scales as  $\sim \mu/r^3$ , with  $r$  being the stellar radius (see Eq. (32)). The

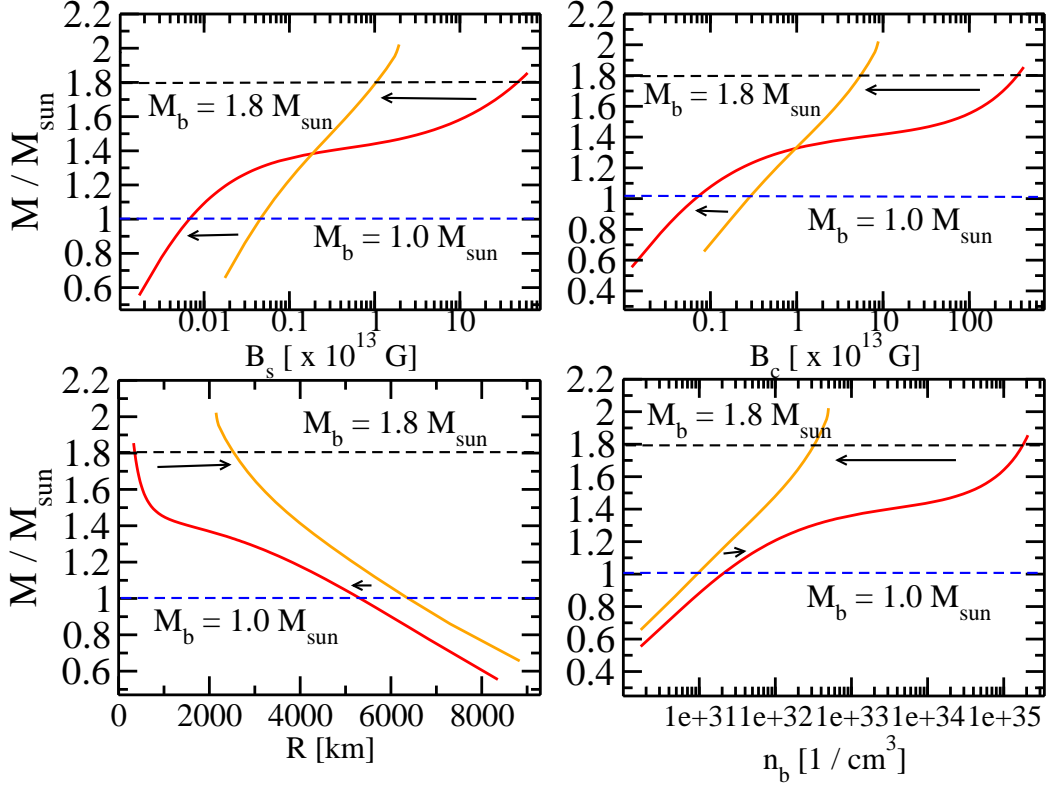


FIG. 6. (Color online) Global properties of magnetized white dwarfs for two different (sample) magnetic dipole moments,  $\mu = 0.5 \times 10^{34} \text{ Am}^2$  (red line) and  $\mu = 4.0 \times 10^{34} \text{ Am}^2$  (orange line).  $M$  denotes the gravitational mass,  $B_S$  the magnetic field at the surface,  $B_c$  the magnetic field at the center,  $R$  the equatorial radius, and  $n_b$  the baryon number density. The horizontal lines represent white dwarfs with fixed baryon masses of  $M_B = 1.00 M_\odot$  (bottom), and  $M_B = 1.80 M_\odot$  (top). The arrows indicate the paths of these white dwarfs in case of a magnetic field reduction (see text for details).

locations of stars with fixed baryon masses of  $M_B = 1.00 M_\odot$  and  $M_B = 1.80 M_\odot$  are shown in Fig. 6 by dashed horizontal lines. According to Eq. (32), the magnetic field is determined by the size of the star along the curves with  $\mu = \text{const}$ . However, along the lines with fixed baryon masses, the strength of the magnetic field is a combination of the magnetic dipole moment  $\mu$  and the stellar radius  $r$ .

Next, we discuss the behavior of the magnetic dipole moments of white dwarfs whose magnetic fields are weakening. From the  $M$  versus  $B_s$  and  $M$  versus  $B_c$  relationships shown in Fig. 6 (top panels), one sees that two different scenarios are possible, depending on the star mass and on the magnetic field strengths of white dwarfs. If located above the crossing point of the  $\mu = 0.5 \times 10^{34} \text{ Am}^2$  (red line) and  $\mu = 4.0 \times 10^{34} \text{ Am}^2$  (orange line) curve, white dwarfs with weakening magnetic fields would be evolving from right to left in the two upper panels of Fig. 6, as shown (back arrow) for a white dwarf with a constant baryon number of  $M_B = 1.80 M_\odot$ . The magnetic dipole moment of such white dwarfs would increase, from  $\mu = 0.5 \times 10^{34} \text{ Am}^2$  to  $\mu = 4.0 \times 10^{34} \text{ Am}^2$  for the sample star shown in Fig. 6. This is accompanied by an increase in the stellar radius (see  $M$  versus  $R$  diagram) and a decrease in the central baryon density (see  $M$  versus  $n_b$  diagram). The situation is reversed for white dwarfs located below the the crossing. For such white dwarfs, a reduction of the magnetic field is accompanied by a decrease of the magnetic dipole moment, as shown in Fig. 6 for a sample white dwarf with a constant baryon mass of  $M_B = 1.00 M_\odot$  (black arrows). In this case, white dwarfs become smaller and therefore more dense at the center (see  $M$  versus  $R$  and  $M$  versus  $n_b$  diagrams shown in Fig. 6).

As discussed just above (Fig. 6), the equatorial radii of white dwarfs located above the crossing point increase as their magnetic fields are getting smaller. The increases in radius (at a fixed baryon mass) is due to the Lorentz force. However, the stellar magnetic field scales as  $\mu/r^3$ . This means that for a star with a mass of  $M_B = 1.80 M_\odot$ , the increase in the magnetic dipole moment,  $\mu$ , is canceled by the increase in the radius, reducing the magnetic field. This is the opposite of what is expected for stars with lower masses. For example, a star with  $M_B = 1.00 M_\odot$  decreases its magnetic dipole moment and its radius. However, in this case, the decrease in the radius is not enough to cancel the reduction in  $\mu$ . The net result is a decrease of the magnetic field. This can be understood by looking at the variation in the circular equatorial radius of the stars with  $M_B = 1.80 M_\odot$  and  $M_B = 1.00 M_\odot$ . For the latter, the change

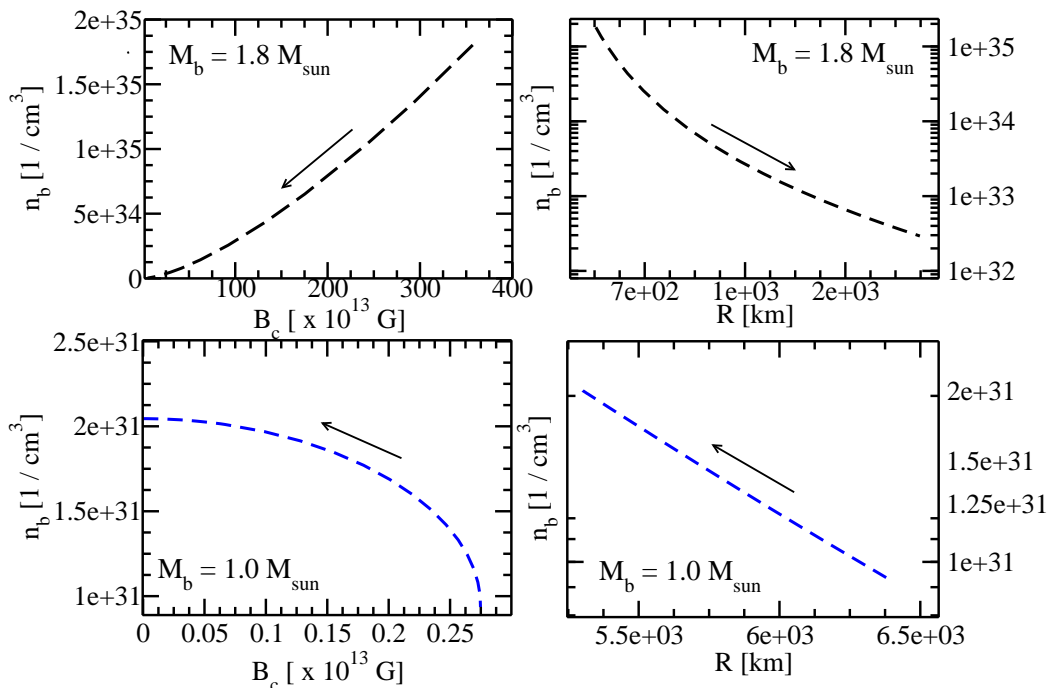


FIG. 7. Central baryon number density,  $n_b$ , as a function of central magnetic field strength,  $B_c$ , and equatorial radius,  $R$ , of magnetized white dwarfs with fixed baryon masses of  $M_B = 1.00 M_\odot$  and  $M_B = 1.80 M_\odot$ . The arrows refer to changes in  $n_b$  and  $R$  for weakening magnetic fields.

in radius is much smaller than the radial change for the  $M_B = 1.80 M_\odot$  star, for a change in the magnetic dipole moment of  $|\Delta\mu| = 3.5 \times 10^{34} \text{ Am}^2$ .

In Fig. 7, we show the global properties of two white dwarfs with fixed baryon masses of  $M_B = 1.00 M_\odot$  and  $M_B = 1.80 M_\odot$ . The top panels show the central baryon density as a function of the central magnetic field (top-left left panel) and the circular equatorial radius (top-right panel) for a white dwarf with  $M_B = 1.80 M_\odot$ . For such stars, as the magnetic field decreases, the central baryon density becomes smaller due to the fact that the radius is increasing. On the other hand, for lighter white dwarfs, with a mass of  $M_B = 1.00 M_\odot$ , the central baryon number density increases as the magnetic field decreases, since the stellar radius is getting smaller.

## VI. SUMMARY

In this work, we presented axisymmetric and stationary models of magnetized white dwarfs obtained by solving the Einstein-Maxwell equations self-consistently and taking into stability considerations related to neutronization due to electron capture reactions as well as pycnonuclear fusion reactions among carbon nuclei in the cores of white dwarfs.

We investigated also the influence of magnetic fields on the structure of white dwarfs. This is an important problem, since super-massive magnetized WD's, whose existence is partially supported by magnetic forces, could simplify the explanation of observed ultra-luminous explosions of supernovae Type Ia. The Lorentz force induced by strong magnetic fields breaks the spherical symmetry of stars and increases their masses, since the force acts in the radial outward direction against the inwardly directed gravitational pull.

In this paper, we make use of an equation of state for a degenerate electron gas with electron-ion interactions (body-centered-cubic lattice structure) to describe the matter inside of white dwarfs. We have shown that the equation of state becomes softer if nuclear lattice contributions are included in addition to the electron pressure. This is due to the fact that the repulsive force between electrons is smaller in the presence of an ionic lattice, causing a softening of the equation of state (see Fig. 1). We note that the density thresholds for pycnonuclear fusion reactions and inverse  $\beta$ -reactions are reduced when magnetic fields are present in the stellar interior, as can be seen in Table III.

We have shown that the masses of white dwarfs increase up to  $M = 2.14 M_\odot$  (with a corresponding magnetic dipole moment of  $\mu = 2.0 \times 10^{34} \text{ Am}^2$  (see, e.g., Fig. 4) if microphysical instabilities are considered. This star has an equatorial radius of  $\sim 1100 \text{ km}$  with magnetic fields of  $B_c = 3.85 \times 10^{14} \text{ G}$  and  $B_s = 7.21 \times 10^{13} \text{ G}$  at the center and at the stellar surface, respectively. For this white dwarf, the ratio between the magnetic pressures and the matter

pressure at the center is 0.789. Although the surface magnetic fields obtained here are higher than the observed ones for white dwarfs, these figures provide an idea of the maximum possible magnetic field strength that can be reached inside of these objects, and may also be used to assess the effects of strong magnetic fields on both the microphysics and the global structure of magnetized white stars.

The maximum magnetic field found in this work is an order of magnitude smaller than that of Ref. [22]. This is because we modeled the stellar interior with a more realistic equation of state than just a simple electron gas, and we considered the density threshold for pycnonuclear fusion reactions for a 10 Gyrs fusion reaction time scale, which restricts the central density of white dwarfs to  $\sim 9.25 \times 10^9$  g/cm<sup>3</sup> (see Table III), limiting the stellar masses and, therefore, their radii, which for very massive and magnetized white dwarfs cannot be smaller than  $R \sim 1100$  km. However, it is important to mention that the pycnonuclear reaction time scales are somewhat uncertain. In our case, for example, we have a factor of uncertainty of approximately 3.5 in the calculation of the astrophysical S-factor (see Refs. [57, 58]).

Our results show that the surface magnetic field,  $B_s$ , is about one order of magnitude smaller than the magnetic field reached at the stellar center,  $B_c$ . If the magnetic field weakens for massive white dwarfs, we found that the magnetic dipole moments of such stars may increase (Fig. 6), which is due to the fact that, for a fixed baryon mass, the magnetic field is determined by the interplay between the magnetic dipole moment and the stellar radius. The situation is reversed for less massive white dwarfs, for which smaller the magnetic fields imply smaller stellar magnetic dipole moments. The radii of massive (light) white dwarfs are found to increase (decrease) for decreasing central magnetic fields (Fig. 7). This opens up the possibility that massive white dwarfs, with central magnetic fields greater than  $B \sim 10^{13}$  G, increase their magnetic fields through continued compression. This phenomenology differs from previous studies carried out for magnetic fields less than  $\sim 10^{13}$  G [26, 41], where an increase of the central magnetic field was found to make stars less dense and therefore bigger in size.

We note that stellar configurations which contain only poloidal magnetic fields (no toroidal component) are unstable (see, e.g., [67–69]). Moreover, according to Ref. [70], many different mechanisms can affect the magnetic fields and their distributions inside of white dwarfs. In this work, in the framework of a fully general relativistic treatment, we model the properties of magnetized white dwarfs with purely poloidal magnetic field components. Although this is not the most general magnetic field profile, and a dynamical stability of these stars still needs to be addressed, magnetic fields considerably increase the masses of white dwarfs, even when microphysical instabilities are considered. As a consequence, such white dwarfs ought to be considered as possible candidates of super-Chandrasekhar white dwarfs, thereby contributing to our understanding of superluminous type-Ia supernovae.

Lastly, we note that for a typical magnetic field value of  $\sim 10^{14}$  G and a density of  $\sim 10^9$  g/cm<sup>3</sup>, we obtain an Alfvén velocity of  $v = 10^9$  cm/s, which, for a white dwarf with a typical radius of  $R = 1500$  km, leads to an Alfvén crossing time of  $\sim 0.1$  s [71–73]. This is close to the hydrostatic equilibration time of white dwarfs. As a consequence, although magnetized white dwarfs seem to be short-lived stars, they might still be supported by magnetic fields. Our results represent magnetostatic equilibrium conditions. The stability analysis of such systems is beyond the scope of this study, which constitutes a first step toward a more complete discussion of the possible existence of super-Chandrasekhar white dwarfs. Studies which address issues such as the role of different (poloidal and toroidal) magnetic field configurations, stellar rotation, and different compositions of the stellar cores will be presented in a series of forthcoming papers.

## VII. ACKNOWLEDGMENTS

We acknowledge financial support from the Brazilian agencies CAPES, CNPq, and we would like to thank FAPESP for financial support under the thematic project 13/26258-4 B. Franzon acknowledges support from CNPq/Brazil, DAAD and HGS-HIRE for FAIR. S. Schramm acknowledges support from the HIC for FAIR LOEWE program. F. Weber is supported by the National Science Foundation (USA) under Grant PHY-1411708.

- 
- [1] F. Weber, *Pulsars as astrophysical laboratories for nuclear and particle physics* (CRC Press, 1999).
  - [2] S. L. Shapiro and S. A. Teukolsky, *Black holes, white dwarfs and neutron stars: the physics of compact objects* (2008).
  - [3] N. K. Glendenning, *Compact stars: Nuclear physics, particle physics and general relativity* (Springer Science & Business Media, 2012).
  - [4] L. G. Althaus, J. A. Panei, M. M. M. Bertolami, E. Garca-Berro, A. H. Corsico, A. D. Romero, S. Kepler, and R. D. Rohrmann, *The Astrophysical Journal* **704**, 1605 (2009).
  - [5] G. Arutyunyan, D. Sedrakyan, and É. Chubaryan, *Soviet Astronomy* **15**, 390 (1971).
  - [6] K. Boshkayev, J. A. Rueda, R. Ruffini, and I. Siutsou, *The Astrophysical Journal* **762**, 117 (2013).

- [7] J. B. Hartle, *The Astrophysical Journal* **150**, 1005 (1967).
- [8] J. G. Coelho, R. M. Marinho, M. Malheiro, R. Negreiros, D. L. Cáceres, J. A. Rueda, and R. Ruffini, *apj* **794**, 86 (2014), arXiv:1306.4658 [astro-ph.SR].
- [9] R. V. Lobato, M. Malheiro, and J. G. Coelho, *International Journal of Modern Physics D* **25**, 1641025 (2016), <http://www.worldscientific.com/doi/pdf/10.1142/S021827181641025X>.
- [10] B. Mukhopadhyay and A. Rao, *Journal of Cosmology and Astroparticle Physics* **2016**, 007 (2016).
- [11] Y. Terada, T. Hayashi, M. Ishida, K. Mukai, T. u. Dotani, S. Okada, R. Nakamura, S. Naik, A. Bamba, and K. Makishima, *Publ. Astron. Soc. Jap.* **60**, 387 (2008), arXiv:0711.2716 [astro-ph].
- [12] D. Reimers, S. Jordan, D. Koester, N. Bade, T. Kohler, and L. Wisotzki, *Astron. Astrophys.* **311**, 572 (1996), arXiv:astro-ph/9604104 [astro-ph].
- [13] G. D. Schmidt and P. S. Smith, *Astrophys. J.* **448**, 305 (1995).
- [14] J. C. Kemp, J. B. Swedlund, J. D. Landstreet, and J. R. P. Angel, *Astrophys. J.* **161**, L77 (1970).
- [15] A. Putney, *The Astrophysical Journal Letters* **451**, L67 (1995).
- [16] J. Angel, *Annual Review of Astronomy and Astrophysics* **16**, 487 (1978).
- [17] L. Mestel, *Stellar magnetism*, Vol. 154 (OUP Oxford, 2012).
- [18] L. D. Landau, E. M. Lifshitz, J. B. Sykes, J. S. Bell, and M. E. Rose, *Physics Today* **11**, 56 (1958).
- [19] U. Das and B. Mukhopadhyay, *Journal of Cosmology and Astroparticle Physics* **2014**, 050 (2014).
- [20] P. Bera and D. Bhattacharya, *Monthly Notices of the Royal Astronomical Society* **445**, 3951 (2014).
- [21] P. Bera and D. Bhattacharya, *Monthly Notices of the Royal Astronomical Society* **456**, 3375 (2016).
- [22] B. Franzon and S. Schramm, *Phys. Rev. D* **92**, 083006 (2015), arXiv:1507.05557 [astro-ph.SR].
- [23] B. Franzon and S. Schramm, (2016), 10.1093/mnras/stx397, [*Mon. Not. Roy. Astron. Soc.* 467,4484(2017)], arXiv:1609.00493 [astro-ph.SR].
- [24] U. Das and B. Mukhopadhyay, *Journal of Cosmology and Astroparticle Physics* **2015**, 016 (2015).
- [25] S. Chandrasekhar, *An Introduction to the Study of Stellar Structure* (Chicago : Univ. Chicago Press, 1939).
- [26] I.-S. Suh and G. Mathews, *The Astrophysical Journal* **530**, 949 (2000).
- [27] J. M. Silverman, M. Ganeshalingam, W. Li, A. V. Filippenko, A. A. Miller, and D. Poznanski, *Monthly Notices of the Royal Astronomical Society* **410**, 585 (2011).
- [28] R. A. Scalzo *et al.*, *Astrophys. J.* **713**, 1073 (2010), arXiv:1003.2217 [astro-ph.CO].
- [29] D. A. Howell *et al.* (SNLS), *Nature* **443**, 308 (2006), arXiv:astro-ph/0609616 [astro-ph].
- [30] M. Hicken, P. M. Garnavich, J. L. Prieto, S. Blondin, D. L. DePoy, R. P. Kirshner, and J. Parrent, *Astrophys. J.* **669**, L17 (2007), arXiv:0709.1501 [astro-ph].
- [31] M. Yamanaka *et al.*, *Astrophys. J.* **707**, L118 (2009), arXiv:0908.2059 [astro-ph.HE].
- [32] S. Taubenberg, S. Benetti, M. Childress, R. Pakmor, S. Hachinger, P. Mazzali, V. Stanishev, N. Elias-Rosa, I. Agnoletto, F. Bufano, *et al.*, *Monthly Notices of the Royal Astronomical Society* **412**, 2735 (2011).
- [33] S. O. Kepler, S. J. Kleinman, A. Nitta, D. Koester, B. G. Castanheira, O. Giovannini, A. F. M. Costa, and L. Althaus, *Monthly Notices of the Royal Astronomical Society* **375**, 1315 (2007), <http://mnras.oxfordjournals.org/content/375/4/1315.full.pdf+html>.
- [34] M. Ilkov and N. Soker, *Monthly Notices of the Royal Astronomical Society* **419**, 1695 (2012), <http://mnras.oxfordjournals.org/content/419/2/1695.full.pdf+html>.
- [35] R. Moll, C. Raskin, D. Kasen, and S. Woosley, *Astrophys. J.* **785**, 105 (2014), arXiv:1311.5008 [astro-ph.HE].
- [36] S. Ji, R. T. Fisher, E. Garca-Berro, P. Tzeferacos, G. Jordan, D. Lee, P. Lorn-Aguilar, P. Cremer, and J. Behrends, *The Astrophysical Journal* **773**, 136 (2013).
- [37] D. R. van Rossum, R. Kashyap, R. Fisher, R. T. Wollaeger, E. Garca-Berro, G. Aznar-Sigun, S. Ji, and P. Lorn-Aguilar, *The Astrophysical Journal* **827**, 128 (2016).
- [38] H. Liu, X. Zhang, and D. Wen, *Physical Review D* **89**, 104043 (2014).
- [39] U. Das and B. Mukhopadhyay, *Modern Physics Letters A* **29**, 1450035 (2014).
- [40] D. Adam, *Astronomy and Astrophysics* **160**, 95 (1986).
- [41] J. P. Ostriker and F. Hartwick, *The Astrophysical Journal* **153**, 797 (1968).
- [42] S. Subramanian and B. Mukhopadhyay, *Monthly Notices of the Royal Astronomical Society* **454**, 752 (2015), <http://mnras.oxfordjournals.org/content/454/1/752.full.pdf+html>.
- [43] P. Bera and D. Bhattacharya, *Monthly Notices of the Royal Astronomical Society* **456**, 3375 (2016).
- [44] U. Das and B. Mukhopadhyay, *Physical Review D* **86** (2012), 10.1103/PhysRevD.86.042001.
- [45] J. G. Coelho, R. M. Marinho, M. Malheiro, R. Negreiros, D. L. Cceres, J. A. Rueda, and R. Ruffini, *The Astrophysical Journal* **794**, 86 (2014).
- [46] N. Chamel, A. F. Fantina, and P. J. Davis, *Physical Review D* **88** (2013), 10.1103/PhysRevD.88.081301.
- [47] E. E. Salpeter, *The Astrophysical Journal* **134**, 669 (1961).
- [48] N. Chamel and A. F. Fantina, *Phys. Rev. D* **92**, 023008 (2015).
- [49] P. Bera and D. Bhattacharya, *Mon. Not. Roy. Astron. Soc.* **445**, 3951 (2014), arXiv:1405.2282 [astro-ph.SR].
- [50] T. Hamada and E. E. Salpeter, *The Astrophysical Journal* **134**, 683 (1961).
- [51] M. Wang, G. Audi, A. H. Wapstra, F. G. Kondev, M. MacCormick, X. Xu, and B. Pfeiffer, *Chinese Physics C* **36**, 1603 (2012).
- [52] G. Audi, M. Wang, A. H. Wapstra, F. G. Kondev, M. MacCormick, X. Xu, and B. Pfeiffer, *Chinese Physics C* **36**, 1287 (2012).
- [53] J. M. Pearson, S. Goriely, and N. Chamel, *Physical Review C* **83** (2011), 10.1103/PhysRevC.83.065810.

- [54] N. Chamel, E. Molter, A. Fantina, and D. P. Arteaga, *Physical Review D* **90** (2014), 10.1103/PhysRevD.90.043002.
- [55] G. Gamow, *Physical Review* **55**, 718 (1939).
- [56] P. Haensel, A. Y. Potekhin, and D. G. Yakovlev, *Neutron stars 1: Equation of state and structure*, Vol. 326 (Springer Science & Business Media, 2007).
- [57] L. R. Gasques, A. V. Afanasjev, E. F. Aguilera, M. Beard, L. C. Chamon, P. Ring, M. Wiescher, and D. G. Yakovlev, *Physical Review C* **72** (2005), 10.1103/PhysRevC.72.025806.
- [58] D. G. Yakovlev, L. R. Gasques, A. V. Afanasjev, M. Beard, and M. Wiescher, *Physical Review C* **74** (2006), 10.1103/PhysRevC.74.035803.
- [59] M. A. Cândido Ribeiro, L. C. Chamon, D. Pereira, M. S. Hussein, and D. Galetti, *Phys. Rev. Lett.* **78**, 3270 (1997).
- [60] L. C. Chamon, D. Pereira, M. S. Hussein, M. A. Cândido Ribeiro, and D. Galetti, *Phys. Rev. Lett.* **79**, 5218 (1997).
- [61] S. Bonazzola, E. Gourgoulhon, M. Salgado, and J. Marck, *Astronomy and Astrophysics* **278**, 421 (1993).
- [62] M. Bocquet, S. Bonazzola, E. Gourgoulhon, and J. Novak, *Astron. Astrophys.* **301**, 757 (1995), arXiv:gr-qc/9503044 [gr-qc].
- [63] B. Franzon, V. Dexheimer, and S. Schramm, *Monthly Notices of the Royal Astronomical Society* **456**, 2937 (2016).
- [64] B. Franzon, V. Dexheimer, and S. Schramm, *Phys. Rev.* **D94**, 044018 (2016), arXiv:1606.04843 [astro-ph.HE].
- [65] B. Franzon, R. O. Gomes, and S. Schramm, (2016), 10.1093/mnras/stw1967, arXiv:1608.02845 [astro-ph.HE].
- [66] E. Gourgoulhon, *3+ 1 formalism in general relativity: bases of numerical relativity*, Vol. 846 (Springer Science & Business Media, 2012).
- [67] C. Armaza, A. Reisenegger, and J. A. Valdivia, *The Astrophysical Journal* **802**, 121 (2015).
- [68] J. Mitchell, J. Braithwaite, A. Reisenegger, H. Spruit, J. Valdivia, and N. Langer, *Monthly Notices of the Royal Astronomical Society* **447**, 1213 (2015).
- [69] J. Braithwaite, *Astronomy & Astrophysics* **453**, 687 (2006).
- [70] P. Goldreich and A. Reisenegger, *The Astrophysical Journal* **395**, 250 (1992).
- [71] R. H. Durisen, *The Astrophysical Journal* **183**, 215 (1973).
- [72] D. Yakovlev and V. Urpin, *Soviet Astronomy* **24**, 303 (1980).
- [73] A. Cumming, *Monthly Notices of the Royal Astronomical Society* **333**, 589 (2002).